

Supporting Information

Flexible PVDF membranes with exceptional robust superwetting surface for continuous separation of oil/water emulsions

Zhu Xiong^{†‡}, Haibo Lin^{†‡}, Fu Liu^{†*}, Peng Xiao[†], Ziyang Wu[†], Tiantian Li[†],
Dehong Li[†]

Based on the preparation route of **Figure S1a**, some characteristic peaks at 3008~2856 cm^{-1} , 1643 cm^{-1} , 1384 cm^{-1} , 1241 cm^{-1} , 1211 cm^{-1} , 1151 cm^{-1} and 1068 cm^{-1} ascribing to the -CH₂-, -CH₃-, and -CF- of FOTS was distinctly appeared in the FTIR spectra of FOTS-g-TiO₂ nanoparticles (**Figure S1b**), indicating some FOTS molecules grafted onto the surface of TiO₂ nanoparticles. TGA was carried out to calculate the FOTS grafting ratio at a heating rate of 10 °C min⁻¹ over a range of 80 °C~700 °C under nitrogen atmosphere. As shown in **Figure S1c**, the final loss weight of the pristine TiO₂ and FOTS-g-TiO₂ nanoparticles was ~3% and ~12 wt%, respectively. Thus, we can obtain that the grafting yield of the FOTS was about 9 wt% in FOTS-g-TiO₂ nanoparticles. With the modification of FOTS, the water contact angle of TiO₂ nanoparticle coating on the glass plate could maintain at 154 °C for at least 60 s, which exhibited the excellent superhydrophobicity. But for the pristine TiO₂ nanoparticle, its water contact angle was quickly decreased from 105 to 31 °C in only 5 s, indicating the good hydrophilicity. Thus, we can conclude that the superhydrophobicity of the modified TiO₂ nanoparticles was fabricated by the grafted FOTS.

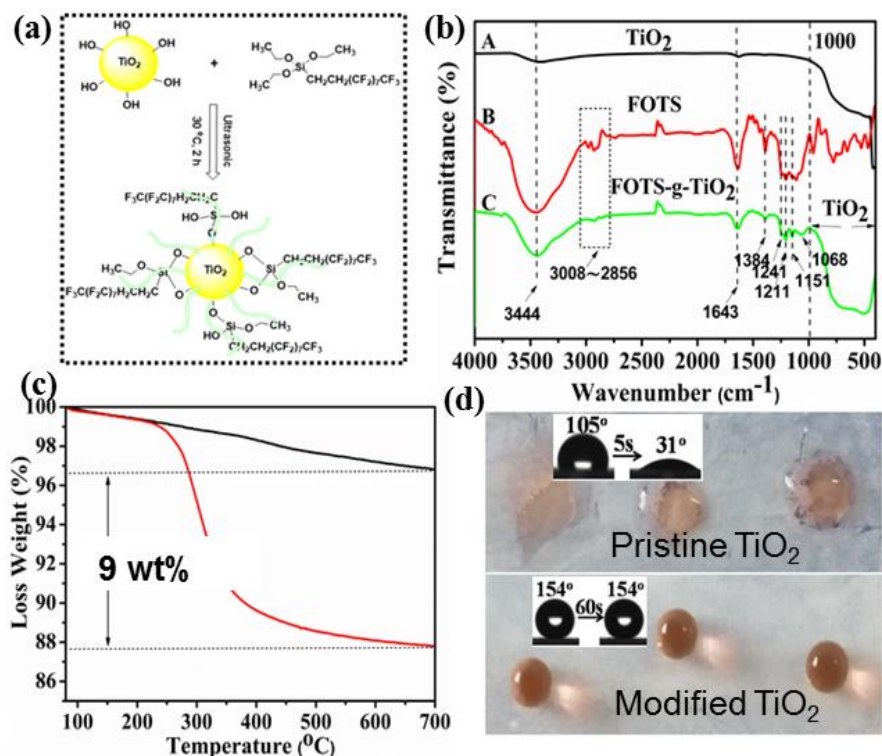


Figure S1. (a) The synthetic route of the superhydrophobic TiO₂ nanoparticles; (b) The FTIR, (c) TGA and (d) contact angle of the TiO₂ nanoparticles with and without modification.

There are discrete grooves of 50~100 μm in diameter disorderly distributed in the surface of the pristine PVDF membrane as shown in **Figure S2a**. From the higher magnification images, the pristine PVDF membrane surface is rather raspy with peak-to-peak roughness $\sim 12.4 \mu\text{m}$ as shown in **Figure S2a₂** and **Figure S2c**. Meanwhile, cilia-like nano-fibrils are stretching out of the surface, which could be regarded as the nano-/micro- multiscale plant roots as observed in **Figure S2a₁**, **a₂**. This hierarchical surface offered the pristine PVDF membrane with excellent superhydrophobicity with the water contact angle (CA) about 153° in **Figure S2c**. As shown in **Figure S2b**, **b₁**, a tight TiO₂ nanoparticle coating was inlaid on the surface of the pristine PVDF membrane including the discrete grooves. Whilst the image was enlarged as shown in **Figure S2b₂**, almost all TiO₂ nanoparticles are captured, confined and caged by the raspy fibrils and microspores of the pristine PVDF membrane. The newly assembled TiO₂ interface with the roughness of 7.6

μm exhibited superhydrophobicity with the contact angle of $\sim 154^\circ$ (**Figure S2e**). In contrast with the perfluorosilane TiO_2 , the pristine TiO_2 could also form a layer on the PVDF membrane surface with the roughness of $7.8 \mu\text{m}$. However, the corresponding surface exhibited the hydrophilicity with the contact angle of $\sim 36^\circ$ as demonstrated in **Figure S2d**. These results revealed that the superhydrophobicity of the interface strengthened PVDF membrane was endowed by FOTS modified TiO_2 nanoparticles.

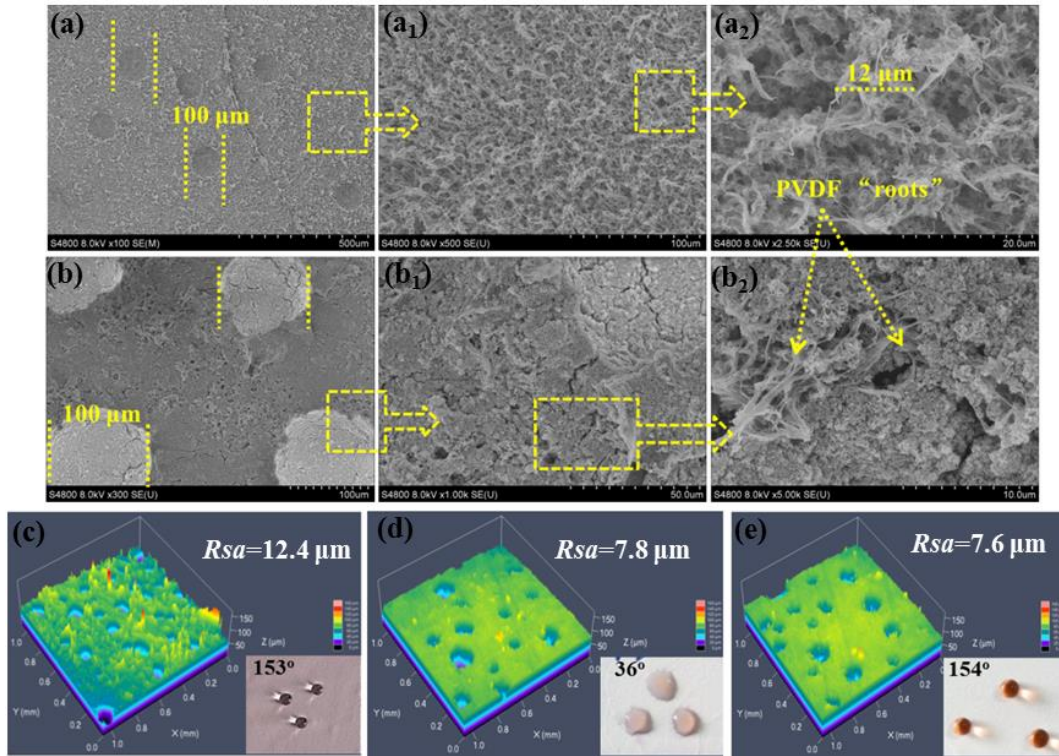


Figure S2. (a)-(a₂) SEM images of the pristine PVDF membrane with different scales: $500 \mu\text{m}$ (a), $100 \mu\text{m}$ (a₁), $20 \mu\text{m}$ (a₂). (b)-(b₂) SEM images of the rigid PVDF membrane with different scales: $100 \mu\text{m}$ (b), $50 \mu\text{m}$ (a₁), $10 \mu\text{m}$ (a₂). (c)-(e) 3D images of the soft PVDF membrane, PVDF membrane with the pristine TiO_2 coating, and the PVDF membrane with the FOTS-g- TiO_2 coating. The insert photographs are the water contact angle.

In **Figure S3a** and **Table S1**, the characteristic peaks at 1403 , 1383 , 1211 , 1180 , 1151 , and 1068 cm^{-1} attributing to the $-\text{CF}-$ were observed for the pristine PVDF membrane. Correspondingly, the characteristic peaks at 686 eV and 285 eV with the mass percentage of $60.2 \text{ wt.}\%$ and $38.9 \text{ wt.}\%$ attributing to the F and C, respectively, were obtained for the special PVDF membrane. After coated by the TiO_2 nanoparticles,

the surface chemical characteristic of PVDF membrane was changed. As observed in **Figure S3b** and **Table S1**, the intensity of -CF- originated from PVDF membrane was reduced with the pristine TiO₂ coating, and the mass percentage of F and C was significantly decreased, and the new peaks at 456 eV and 530 eV attributing to the Ti and O distinctly appeared, indicating the PVDF membrane surface was mainly fabricated by the pristine TiO₂ coating. Furthermore, as seen in **Figure S3c** and **Table S1**, the intensity of -CF- of the PVDF membrane was increased with the FOTS-g-TiO₂ coating in comparison with that of the pristine TiO₂ coating, and the mass percentage of F was significantly increased from 9.9 to 33.0 wt.%, and the new peak at 150 eV and 100 eV attributing to the Si of FOTS appeared, indicating the existence of FOTS on the TiO₂ coating of PVDF membrane surface.

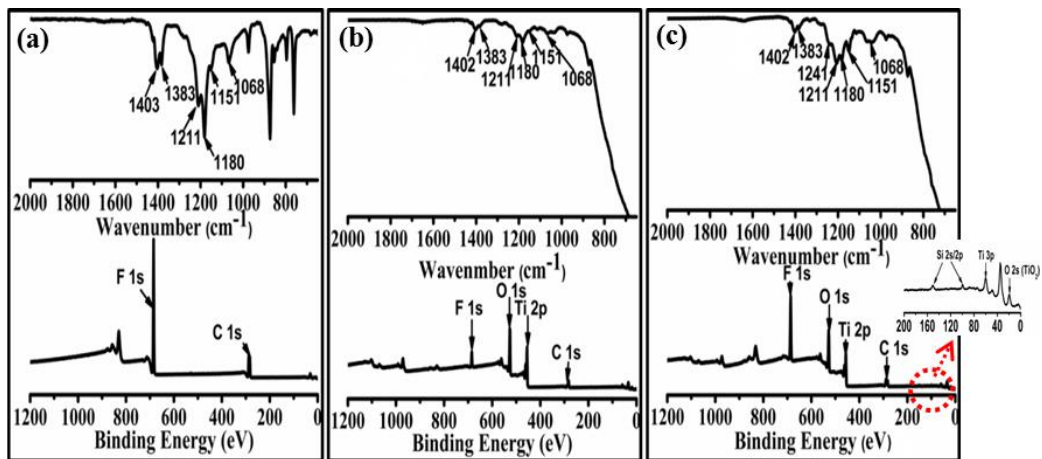


Figure S3. (a)-(c) The FTIR and XPS spectra of the pristine PVDF membrane (a), PVDF membrane manipulated by the pristine TiO₂ nanoparticles (b), PVDF membrane manipulated by the FOTS-g-TiO₂ nanoparticles (c), respectively. The insert picture is the magnified XPS spectra of the PVDF membrane strengthened by the FOTS-g-TiO₂ nanoparticles.

TableS1. Elemental mass percentage obtained from the XPS

Sample	Percentage of components (wt.%)				
	F	O	Ti	C	Si
a	60.2	0.9	0	38.9	0
b	9.9	32.6	42.0	15.5	0
c	33.0	21.5	27.8	14.6	3.1

Note: sample a is the pristine PVDF membrane, sample b is the rigid PVDF membrane decorated by the pristine TiO₂, sample c is the rigid PVDF membrane manipulated by the TOFS-g-TiO₂.

On the other side, the delicate polymeric microstructures are usually subject to the thermal deformation due to the inherent flexibility. Given this, the thermal resistant testing was performed with increasing temperature under 10 MPa. As shown in **Figure S4** and **Movie S7**, the WCA of the soft superhydrophobic PVDF membrane was reduced to 100° under 10 MPa loading pressure at room temperature. With the temperature increasing to 80 °C, WCA was further decreased to about 80°, demonstrating the brittleness of polymeric micro-/nano-structures. In comparison, the WCA of the rigid superhydrophobic PVDF membrane remained around 150° without losing its superhydrophobicity when the temperature is up to 180 °C near the melting temperature of PVDF. Overall, as discussed above, the perfluorosilane TiO₂ interface provided the flexible PVDF membrane with robust superhydrophobic surface withstanding the extremely physical attack.

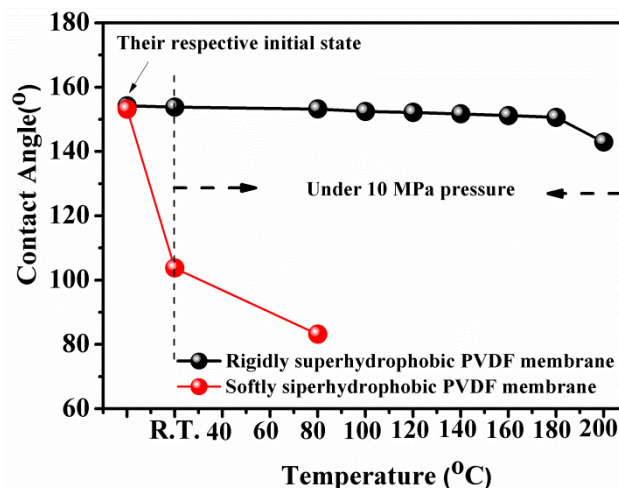


Figure S 4. Contact angle variation of the pristine soft PVDF membrane surfaces and rigid PVDF membrane surface manipulated by perfluorosilaneTiO₂ coating after thermal and pressure tests.

The Separation Efficiency of Water-in-Oil Emulsions: **Figure S5** shows optical microscopy images and size distribution of various water-in-oil emulsions as examples. It is observed that the emulsifier stabilized emulsions are non-transparent and milky, which was caused by the numerous dispersed nano-/micro- droplets. The average size of emulsions is ~4.69 μm, ~1.48 μm, ~2.09 μm, ~5.77 μm, and ~1.90 μm, respectively, for those water-in-oil emulsions involving in toluene, chloroform, n-hexane, soybean oil, and paraffin oil, as exhibited in **Table S2**. The average sizes of the emulsions were calculated by the software Image-ProPlus 6.0 from the optical microscopy images in **Figure S5**. After the dead-end filtration, not a single droplet is observed in the five collected filtrates in the whole optical microscopy images and the five filtrates are all transparent, indicating the effectiveness of the rigid superhydrophobicPVDF membrane for separating various water-in-oil emulsions.

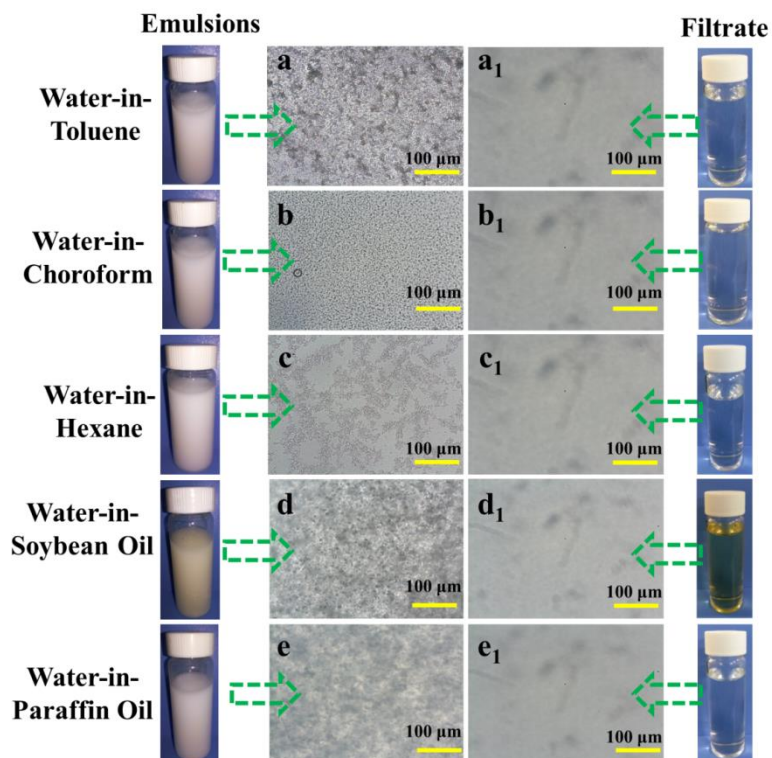


Figure S 5. Optical observation of various water-in-oil emulsions after dead-end separation: (a, a₁) H₂O-in-Toluene emulsion, (b, b₁) H₂O-in-Chloroform emulsion, (c, c₁) H₂O-in-Hexane emulsion, (d, d₁) H₂O-in-Soybean Oil emulsion, (e, e₁) H₂O-in-Paraffin Oil.

Table S2. Nano-/micro- size distribution and viscosity of the five emulsions

Emulsion	H ₂ O-in-Toluene	H ₂ O-in-Chloroform	H ₂ O-in-Hexane	H ₂ O-in-Soybean Oil	H ₂ O-in-Paraffin Oil
Average Size					
Distribution (μm)	4.69	1.48	2.09	5.77	1.90
Viscosity (mPa.s)	0.571	0.647	0.332	50.09	31.36